

MIMO Antenna Based on Metamaterial Frequency Selective Surface

Shengyuan Luo¹, Yingsong Li^{1,2}, Chow-Yen-Desmond Sim³, Yinfeng Xia^{1,*},
and Xiaoguang Liu⁴

¹ College of Information and Communications Engineering, Harbin Engineering University, Harbin 150001, China
*xiayinfeng@hrbeu.edu.cn

² Key Laboratory of Microwave Remote Sensing, National Space Science Center, CAS, Beijing 100190, China

³ Department of Electrical Engineering, Feng Chia University, Taichung 40724, Taiwan

⁴ Electrical and Computer Engineering, University of California, Davis, California 95616, USA

Abstract — In this paper, a metamaterial-based novel antenna-mutual-coupling reduction structure is proposed and demonstrated. The structure consists of a three-layer metamaterial frequency selective surface (MFSS) superstrate with split-ring resonators and metal grids. The MFSS means metamaterial frequency selective surface that has the metamaterial performance along the substrate and the frequency selective characteristic on the normal direction of the antenna array simultaneously. A 1×2 MIMO antenna that has a short edge-to-edge distance ($0.037\lambda_0$) is designed as an illustration to demonstrate the validity of the meta-surface for mutual. When loaded with the proposed MFSS, the mutual coupling between the antenna elements is significantly reduced and the gain of the antenna array is improved by 2.5 dBi.

Index Terms — Frequency selective surface, gain, MIMO antenna array, mutual decoupling.

I. INTRODUCTION

Multiple-input multiple-output (MIMO) technology plays an important role in wireless communication because it has the potential to increase the throughput and capacity of the system [1-3]. Compared with traditional MIMO technology, massive MIMO has the advantages of serving more user terminals and possessing higher energy efficiency and capacity [4-6]. In a massive MIMO communication system, the antenna array usually consists of tens or even hundreds of array elements that are evenly devised with a special contour [4, 5]. For mobile terminal or portable base station that has limited physical space, as the distance between antenna array elements reaches only a fraction of the wavelength, high mutual coupling between them is inevitable.

Recently, many mutual decoupling techniques have been studied [7-19]. Among them, the introduction of

decoupling network/structure such as directional couplers, transmission lines with indirect coupling mechanism, inverted T-slot on ground, and coupled resonators have been reported in [7-9]. As the EBG can exhibit band-gap characteristic to reject the surface wave with high impedance [10], electromagnetic band gap (EBG) and fractal uniplanar compact electromagnetic bandgap (UC-EBG) structure with cross slots, and using periodic mushroom EBG structures have also been investigated to improve the isolation between array elements [10-14]. The defected ground structure (DGS) is also a mature technology for isolation enhancement [15-17]. However, etching a series of periodic DGSs on the metal ground will damage the integrity of the ground plane, which leads to leakage waves and deteriorated radiation patterns of the MIMO antenna array.

In the past decades, metamaterials have received much attention due to its unique characteristics such as negative permittivity, permeability, and reflective index [18-22]. In [18-21], antenna arrays integrated with metamaterial substrate have shown significant size reduction and lower mutual coupling due to the high impedance property of metamaterial. Metamaterial structures can also be suspended above the MIMO antenna to obtain mutual coupling reduction. Even though the suspended metamaterial can significantly enhance the isolation of the MIMO antenna, its matching performance is not ideal as the antennas are no longer matched to free-space medium. Therefore, it is worthy to further study other unique technique that can be integrated with the previous designed MIMO antennas, which can achieve good impedance matching, while still maintaining desirable mutual decoupling performance. Interestingly, in practical engineering applications, the frequency selective surface (FSS) technique is mostly used to reduce radar cross-sectional, realize beam multiplexing and applied as a large bandwidth absorbing

material [23-28], but it is rarely applied to achieve mutual decoupling of array antennas. In recently, an array-antenna decoupling surface has been proposed, but, the mutual decoupling principle is different with the principle in our paper. Partially diffracted waves from the antenna decoupling surface can be controlled to cancel the unwanted coupled waves for the antenna array by using the array-antenna decoupling surface. There are also some meta-surfaces have been proposed in [30, 31], but the impedance of the meta-surfaces in these two papers cannot match well with the antenna array.

In this paper, the technique of integrating the FSS with metamaterial is proposed, in which a single cell (three layers) MFSS structure operating at 5.5 GHz is initially investigated. To further identify its mutual decoupling ability, it is transformed into a metamaterial superstrate (MS) (with 4×6 cells) that is suspended above a conventional 1×2 patch array. Compared with existing mutual decoupling techniques applied to MIMO antenna, this work has the following technical merits:

1. A novel suspended MFSS superstrate is proposed for mutual coupling reduction in MIMO antenna

2. As the suspended MS is composed of a layer of metal grids sandwiched by two layers of split ring resonators (SRRs), it contains the properties of both metamaterial and FSS simultaneously

3. Due to the effects of the FSS, the MFSS can also aid in improving the gain of the antenna array.

4. Because the edge-to-edge distance between two designated antenna array elements in this work can be extremely small ($0.037\lambda_0$), it can therefore be transformed into a low mutual coupling massive MIMO antenna.

5. Compared with the meta-surface in [30] and [31], the MFSS proposed in our paper has a merit that the impedance of this MFSS can match well with the original antenna array, so that it does not need any other options improve the impedance matching between the MFSS and original antenna array due to the frequency selective surface characteristic of the proposed meta-surface.

II. DESIGN OF THE PROPOSED ANTENNA ARRAY

A. Single cell MFSS design

Because the MFSS structure possesses the properties of metamaterial and FSS simultaneously, it is instructive to analyze the MFSS unit cell (Fig. 1) to understand its operating principles. The MFSS unit cell is composed of two stacked square FR4 substrates, each 1.6-mm thick with relative permittivity of 4.4 and loss tangent of 0.02. The substrate is 6 mm•6 mm in size. A 6 mm•6 mm square-ring metal grid with width $t=0.1$ mm is sandwiched between two identical modified SRRs whose split gap $g=0.5$ mm and size length $a_1=5.6$ mm. As shown in Fig.

1, propagation characteristics are first studied along the x-direction. The boundary conditions are set to be perfect magnetic conductors (PMC) and perfect electric conductors (PEC), which used default isotropic homogeneous slab model and leaner polarization, and the default number of modes is 1. The polarization of the incident wave in the waveguide model is the E-field in z polarization with the H-field in y polarization, meanwhile the incident wave of the metamaterial frequency selective surface (MFSS) is TEM mode.

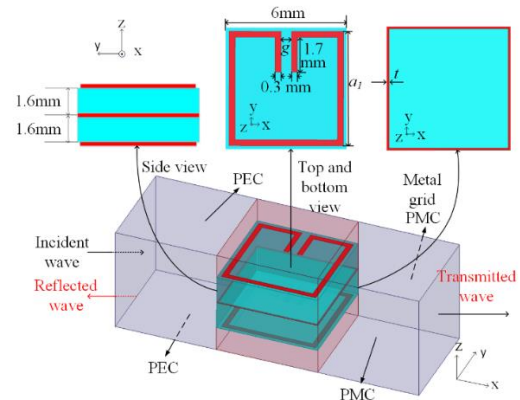


Fig. 1. The geometry and dimensions of the proposed single cell (three-layer) MFSS structure. Top and bottom layers are split ring resonator (SRR) and the middle layer is a metal grid. $a_1=5.6$ mm, $g=0.5$ mm, $t=0.1$ mm.

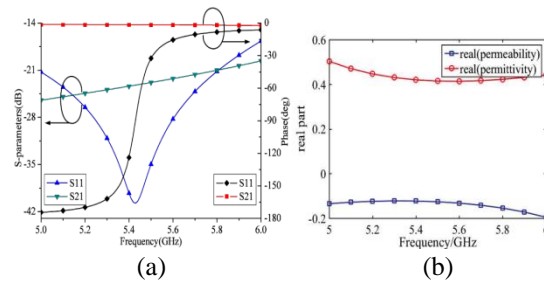


Fig. 2. (a) Simulated amplitude $|S_{11}|$ and $|S_{21}|$ and phase of S_{11} and S_{21} . (b) Extracted permittivity and permeability with respect to frequency.

Figure 2 (a) shows the simulated S-parameters of the structure and Fig. 2 (b) shows the correspondingly extracted permeability and permittivity [32]. From Fig. 2 (a), it can be seen that the phase of S_{11} changes drastically between 5.2 GHz and 5.7 GHz, while the phase of the S_{21} remains almost constant at 0. In the frequency range of 5.2–5.7 GHz, the isolation and return loss are better than 21 dB and 23 dB, respectively. This means that the proposed MFSS unit cell can be expanded and applied as a mutual decoupling device for an antenna array. According to the metamaterial theories, the

resonant frequency and the negative permeability frequency region is determined by the physical size and the gap dimension of the SRRs.

Because the proposed MFSS unit cell shows negative permeability in the 5–6 GHz bands, it is vital to study its transmission characteristics along the z-direction with respect to its physical dimensions (a_1 , g and t). The simulation setup is shown in Fig. 3 (a). As is shown in Fig. 3 (b), the resonant frequency can be linearly decreased from 5.83 GHz to 5.2 GHz by increasing a_1 from 5.5 mm to 5.7 mm. At $a_1=5.6$ mm, a resonant frequency of 5.52 GHz is achieved. Correspondingly, the S_{21} is approximately 1.2 dB [Fig. 3 (c)].

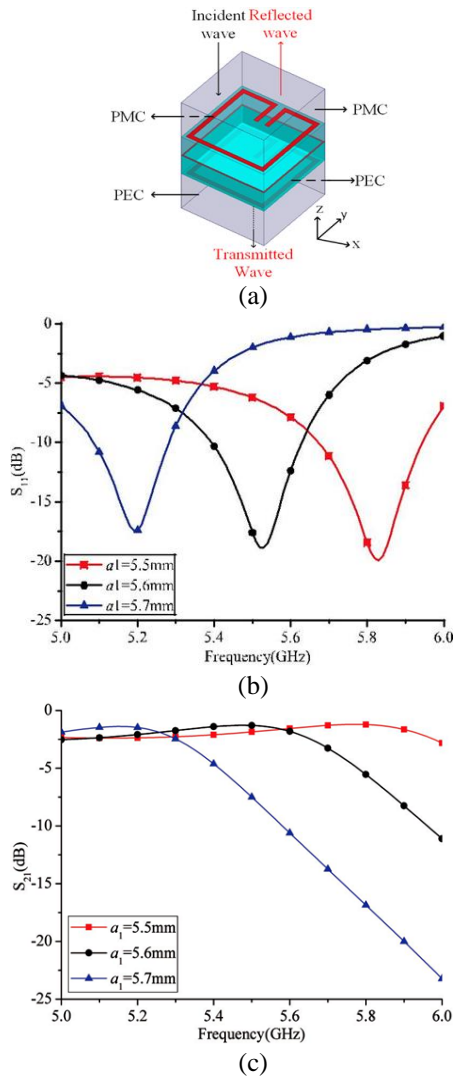


Fig. 3. Simulation setup for incident wave along the z-direction.

Figure 4 (a) and Fig. 4 (b) show the simulated S_{11} when parameters g and t are tuned, respectively. Here, an increasing g from 0.5 mm to 2.5 mm will linearly shift

the resonant frequency from 5.52 GHz to 5.97 GHz. Comparing the two cases where $t=0$ mm, i.e., no metal grids, and $t=0.1$ mm, we can see that the resonant frequencies are similar. However, it is worth mentioning that the resonant frequency of S_{11} for $t=0$ mm will be vanished when the position of the wave ports is the same as in Fig. 1. From the above results, $a_1=5.6$ mm, $g=0.5$ mm and $t=0.1$ mm is selected as the optimized parameters. The equivalent circuits of the MFSS units proposed in this paper has been given in Fig. 5. Due to the effective permeability and the permittivity of the metamaterial were retrieved from the waveguide model, where the incident waves are transmitted on the side direction, therefore, the equivalent circuit given in this paper is correspond to the side excitation. The SRRs on upper and lower planes of this structure can produce an inductance (L_1) and capacitance (C_1), which will result in a band-stop region that has a negative permeability and positive permittivity along the substrate of the MIMO antenna, while the inductance (L_2) in grid and the capacitance (C_1) can form another resonant that results in a band-pass region on the normal direction of the MIMO antenna. Compared with the existing technology of mutual decoupling of the antenna array by using the meta-surface, the meta-surface proposed in this paper does not need any other options to improve the impedance matching between the antenna array and meta-surface. So, if we want to expand this structure into another antenna array, we can apply it directly.

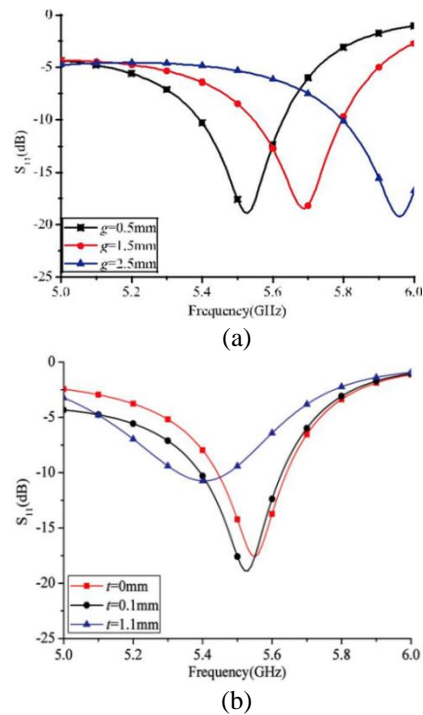


Fig. 4. Simulation setup for incident wave along the z-direction.

According to the simulated results in Fig. 2 (b) and Fig. 3 (b), it can be found that the MFSS means metamaterial frequency selective surface, and this structure owns the metamaterial property along the substrate of the MIMO antenna, meanwhile it has a frequency selective characteristic that can be found from the Fig. 3 (b), which performs a band-pass characteristic along the normal direction of the MIMO antenna. Therefore, the MFSS has another metamaterial characteristic comparing with the normal FSS structure.

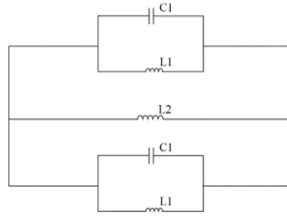


Fig. 5. Equivalent circuit of the MFSS units.

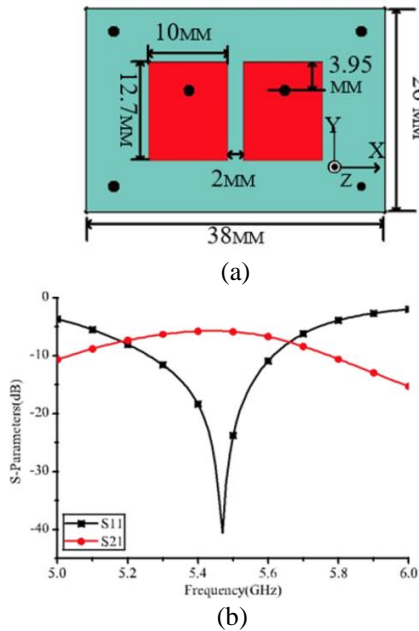


Fig. 6. (a) The geometry and dimensions, and (b) the simulated S-parameters of the proposed reference 1×2 MIMO array.

B. Design of reference 1×2 MIMO antenna array

To validate the mutual coupling reduction performance of the proposed structure, a reference antenna array is first presented Fig. 6 (a). The reference antenna array consists of two identical microstrip antenna elements on a 1.6-mm thick FR4 substrate. The antenna elements are 12.7×10 mm in size and are separated by an edge-to-edge distance of 2 mm. Both array elements are centrally fed by a 50-coaxial probe. Figure 6 (b) shows the simulated S-parameters between the two feedings

of the reference antenna. Although a desirable resonant frequency of 5.48 GHz and a 10-dB impedance bandwidth of 6.25% (5.27-5.61 GHz) are achieved, undesirable coupling of 5.71 dB is observed between the antenna elements due to the tight spacing between them.

C. Design of MIMO antenna array with suspended MFSS

To reduce the mutual coupling between the antenna elements, the proposed MFSS structures are placed as a superstrate 5-mm above the reference antennas. As shown in Fig. 7 (a), the MFSS superstrate is composed of 6×4 MFSS unit cells that collectively cover the reference antennas. The center metal grid of each cell is connected to those of the adjacent cells.

To understand the principle of the MIMO Antenna array with the suspended MFSS, the radiation model is shown in Fig. 7 (b). According to the space electromagnetic wave propagation theory, the plane electromagnetic wave can be expressed as: $A(x) = A_0 e^{i(kx - \omega t)}$.

When a superstrate comprised of the proposed MFSS is placed above the reference MIMO antenna, a negative permeability frequency band region can be achieved, while its corresponding permittivity is positive in this band. Therefore, the wave number in $A_0 e^{jkx}$ can be expressed as:

$$k = k_0 \cdot \sqrt{-|u_r| \cdot |\epsilon_r|} = jk_0 \cdot \sqrt{|u_r| \cdot |\epsilon_r|}, \quad (1)$$

where k is purely imaginary in the negative permeability frequency band. As such, the electromagnetic (EM) wave propagation is not allowed.

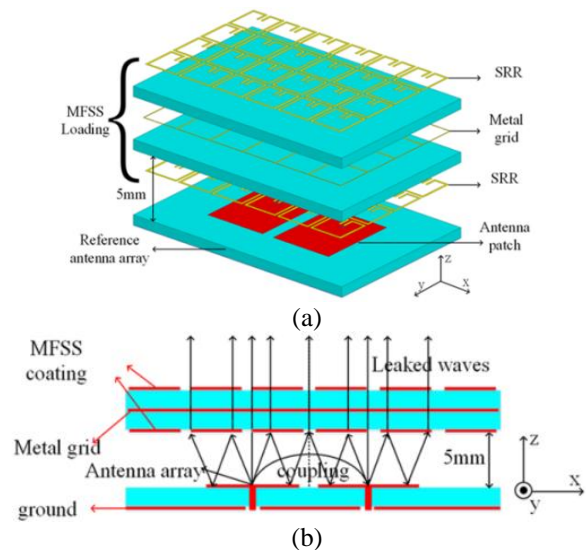


Fig. 7. (a) 3D Illustration and (b) side view of the MFSS loaded 1×2 MIMO array.

To better understand the mutual decoupling mechanism of the MFSS loading, the simulated surface

current distribution without and with MFSS loading are presented in Fig. 8 (a) and Fig. 8 (b), respectively. Without the MFSS loading, one can be seen that a strong induction current appears on the right antenna patch when the left antenna patch was fed by an excitation source. In contrast, with MFSS loading, the induction current on the right antenna patch is very weak. Thus, it is obvious that the suspended MS can effectively reduce the mutual coupling between antenna array elements. Therefore, the surface current distributions of the antenna array with and without the MFSS can fully illustrate the mutual decoupling principle of the antenna array with the MFSS.

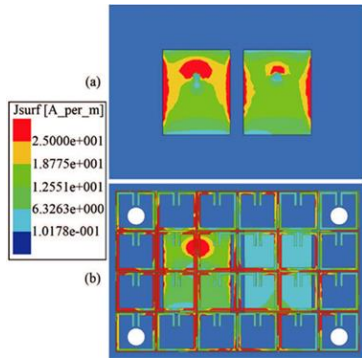


Fig. 8. Surface current distribution of the proposed MIMO antenna array (a) without MFSS loading and (b) with MFSS loading.

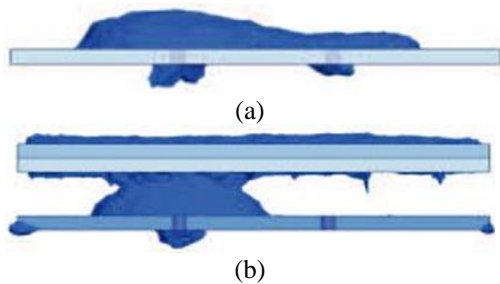


Fig. 9. Simulated electric field distributions in the XOZ-plane for (a) without and (b) with the MFSS loading.

For the FSS, the properties change corresponding to the different distance between antenna array and MFSS. According to the simulation results, when the distance between the antenna array and the MFSS is less than 5 mm, the electromagnetic wave radiated to the MFSS cannot be regarded as a plane wave, which will result in multipath interference in the space between antenna array and MFSS. When the distance between antenna array and MFSS is longer than 5 mm, the negative permeability space of the MFSS cannot cover the antenna array. The decoupling performance is best when the distance between the antenna array and MFSS are suitably selected. Yet, from the simulated surface current distribution of

the proposed MIMO antenna array in Fig. 8, it can be observed the right antenna still exists induced current.

To further explain the above phenomena, the electric field distributions of the proposed MIMO antenna without and with MFSS loading are also shown in Fig. 9 (a) and Fig. 9 (b), respectively. As shown in Fig. 9 (a), without MFSS loading, a large amount of electric field is coupled to the right patch antenna. In contrast, Fig. 9 (b) shows that the electric field is directed toward the broadside direction of the radiating antenna in the presence of MFSS loading.

III. MEASURED PERFORMANCE OF PROPOSED MIMO ANTENNA ARRAY WITH MFSS LOADING

The proposed MIMO antenna array with MFSS loading is fabricated and measured in an anechoic chamber. A photograph of the fabricated device is given in Fig. 10 (a). The measured and simulated S-parameters of the fabricated prototype (with and without MFSS loading) are shown in Fig. 10 (b). With MFSS loading, a measured 10-dB reflection bandwidth of 5.13% (5.32–5.6 GHz) is achieved at a center frequency of 5.46 GHz. The measured S21 is better than 12 dB. Comparing with Fig. 6, we can see that the isolation between the two patch antennas can be enhanced by as much as 20 dB without disturbing the impedance bandwidth. The measurement and simulation generally agree well with each other. The slight difference between the measured and simulated results can be attributed to fabrication tolerances.

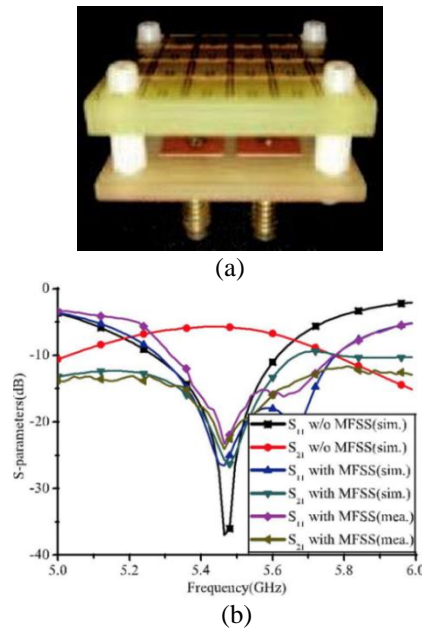


Fig. 10. (a) The photograph of the fabricated device, and (b) the measured and simulated S-parameters of the fabricated prototype.

Figure 11 shows the influence of various distance between MIMO antenna and MFSS. It can be found that when the distance between MIMO antenna and MFSS is 5 mm, the mutual coupling between antenna array elements is the lowest.

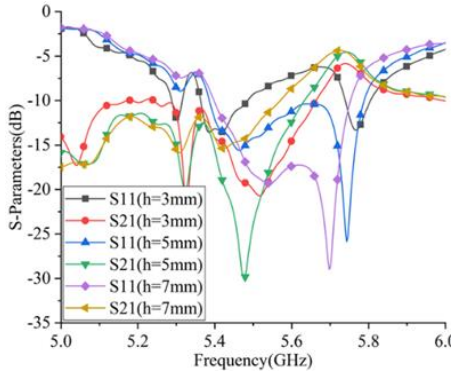


Fig. 11. Simulated S-parameters with influence of various distance h .

Figure 12 shows the measured radiation pattern of the array with MFSS loading. The MFSS loading introduces little perturbation to the radiation characteristics of the antenna array. The measured peak gain with MFSS loading is 7.5 dBi, which represents a 2.5-dBi improvement over the reference array. This is because the MFSS superstrate has aided in concentrating more energy into the band-pass frequency band. The measured radiation efficiency of the proposed antenna array with MFSS loading varies between 67.03% and 74.17% in the 5.35~5.60 GHz range. The calculated peak envelop correlation coefficient (ECC) in the operating band is less than 0.011.

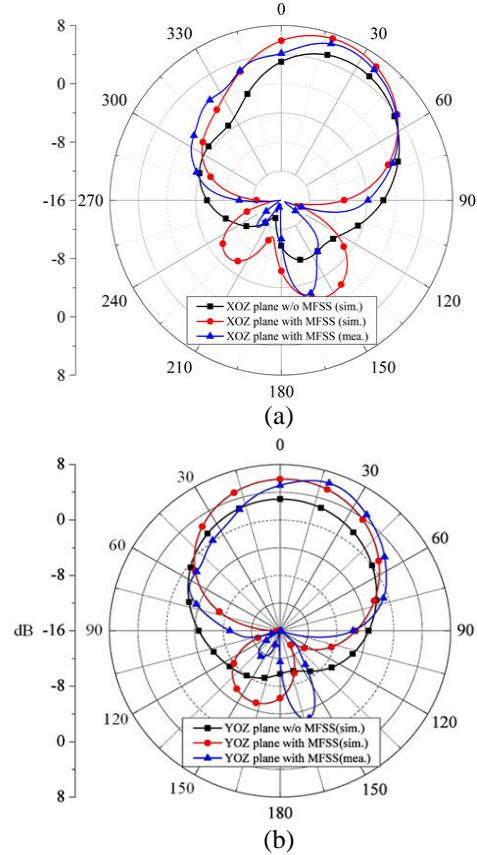


Fig. 12. The simulated and measured radiation patterns of the proposed MIMO antenna array with and without MFSS loading at 5.5 GHz. (a) XOZ plane and (b) YOZ plane.

Table 1: Comparison with the state-of-the-art

Ref.	10-dB BW	Effective Size (c)	Gain/Iso. Enhancement (dB)	Peak ECC/Gain	Eff.
[7]	9.5%	$1.0_{7.5} \times 1.0_{7.5}$	0.33/33	NA/6.55	NA
[10]	2.5%	$0.83_{5.0} \times 0.5_{5.0}$	NA/16	NA/NA	NA
[11]	1.9%	$1.92_{5.82} \times 0.96_{5.82}$	NA/9	NA/NA	NA
[16]	1.9%	$1.48_{5.3} \times 0.86_{5.3}$	0.25/12	NA/NA	NA
[19]	1%	$0.81_{3.475} \times 0.35_{3.475}$	NA/11	NA/4.37	NA
This work	2.7%	$0.69_{5.5} \times 0.47_{5.5}$	2.5/20	0.011/7.5	74.17

*Ref. = Reference, Iso = Isolation, Eff. = Efficiency, BW = Bandwidth.

The performance of the antenna is compared with the state-of-the-art in Table 1. The proposed mutual-coupling-reduction scheme shows smaller physical size, higher gain, and efficiency.

IV. CONCLUSION

A high isolation and gain enhancement MIMO antenna by using the MFSS loading is successfully investigated. The performance of the MIMO antenna

with different dimensions is discussed, optimized and fabricated. From the simulated and measured results, it can be shown that the MFSS has exhibited good metamaterial property and frequency selective characteristic, and the isolation and peak gain of the MIMO antenna are improved by 20 dB and 2.5 dBi with an edge-to-edge distance of only 2 mm. In the future, the embedded decoupling techniques and the other metamaterials can be used for realizing the low coupling

design [33-35]. Also, the MIMO antenna can be used for beamforming using the adaptive techniques [36-39].

ACKNOWLEDGMENT

The authors would like to thank the AnHui Province Key Laboratory of Simulation and Design for Electronic Information System and Shenzhen Sunyield Technologies Co., LTD for help with the measurement. This work was supported in part by the National Key Research and Development Program of China under Grant 2016YFE0111100, the Fundamental Research Funds for the Central Universities 3072020CFT0802, the Key Research and Development Program of Heilongjiang under Grant GX17A016.

REFERENCES

- [1] M. Jensen and J. Wallace, "A review of antennas and propagation for MIMO wireless communications," *IEEE Transactions on Antennas and Propagation*, vol. 52, no. 11, pp. 2810-2824, 2004.
- [2] Y. Li, W. Li, and W. Yu, "A multi-band/UWB MIMO/diversity antenna with an enhanced isolation using radial stub loaded resonator," *Applied Computational Electromagnetics Society Journal*, vol. 28, no. 1, pp. 8-20, 2013.
- [3] L. Kang, H. Li, X. Wang, and X. Shi, "Compact offset microstrip-fed MIMO antenna for band-notched UWB applications," *IEEE Antennas and Wireless Propagation Letter*, vol. 14, pp. 1754-1757, 2015.
- [4] E. Larsson, O. Edfors, F. Tufvesson, and T. Marzetta, "Massive MIMO for next generation wireless systems," *IEEE Communications Magazine*, vol. 52, no. 2, pp. 186-195, 2014.
- [5] L. Lu, G. Li, A. L. Swindlehurst, A. Ashikhmin, and R. Zhang, "An overview of massive MIMO: Benefits and challenges," *IEEE Journal of Selected Topics in Signal Processing*, vol. 8, no. 5, pp. 742-758, 2014.
- [6] M. Wang, Y. Li, H. Zou, M. Peng, and G. Yang, "Compact MIMO antenna for 5G portable device using simple neutralization line structures," *2018 IEEE International Symposium on Antennas and Propagation & USNC/URSI National Radio Science Meeting*, pp. 37-38, Boston, MA, USA, July 2018.
- [7] R. Xia, S. Qu, P. Li, Q. Jiang, and Z. Nie, "An efficient decoupling feeding network for microstrip antenna array," *IEEE Antennas and Wireless Propagation Letters*, vol. 14, pp. 871-874, 2015.
- [8] J. Deng, J. Li, L. Zhao, and L. Guo, "A dual-band inverted-F MIMO antenna with enhanced isolation for WLAN applications," *IEEE Antennas and Wireless Propagation Letters*, vol. 16, pp. 2270-2273, 2017.
- [9] L. Zhao and K. L. Wu, "A dual-band coupled resonator decoupling network for two coupled antennas," *IEEE Transactions on Antennas and Propagation*, vol. 63, no. 7, pp. 2843-2850, 2015.
- [10] X. Yang, Y. Liu, Y. Xu, and S. Gong, "Isolation enhancement in patch antenna array with fractal UC-EBG structure and cross slot," *IEEE Antennas and Wireless Propagation Letters*, vol. 16, pp. 2175-2178, 2017.
- [11] F. Yang and Y. Rahmat-Samii, "Microstrip antennas integrated with electromagnetic band-gap (EBG) structures: A low mutual coupling design for array applications," *IEEE Transactions on Antennas and Propagation*, vol. 51, no. 10, pp. 2936-2946, 2003.
- [12] T. Jiang, T. Jiao, and Y. Li, "Array mutual coupling reduction using L-loading E-shaped electromagnetic band gap structures," *International Journal of Antennas and Propagation*, vol. 2016, Article ID: 6731014, 2016.
- [13] T. Jiang, T. Jiao, and Y. Li, "A low mutual coupling MIMO antenna using periodic multi-layered electromagnetic band gap structures," *Applied Computational Electromagnetics Society Journal*, vol. 33, no. 3, pp. 305-311, 2018.
- [14] Y. Fan, J. Huang, T. Chang, and X. Liu, "A miniaturized four-element MIMO antenna with EBG for implantable medical devices," *IEEE Journal of Electromagnetics, RF and Microwaves in Medicine and Biology*, vol. 2, no. 4, pp. 226-233, 2018.
- [15] D. Hou, S. Xiao, B. Wang, L. Jiang, J. Wang, and W. Hong, "Elimination of scan blindness with compact defected ground structures in microstrip phased array," *IET Microwaves, Antennas & Propagation*, vol. 3, no. 2, pp. 269-275, 2009.
- [16] F. Zhu, J. Xu, and Q. Xu, "Reduction of mutual coupling between closely-packed antenna elements using defected ground structure," *Electronics Letters*, vol. 45, no. 12, pp. 601-602, 2009.
- [17] K. Wei, J. Li, L. Wang, Z. Xing, and R. Xu, "Mutual coupling reduction by novel fractal defected ground structure bandgap filter," *IEEE Transactions on Antennas and Propagation*, vol. 64, no. 10, pp. 4328-4335, 2016.
- [18] R. Hafezifard, M. Naser-Moghaddasi, J. Mohassel, and R. Sadeghzadeh, "Mutual coupling reduction for two closely spaced meander line antennas using metamaterial substrate," *IEEE Antennas and Wireless Propagation Letters*, vol. 15, pp. 40-43, 2016.
- [19] Z. Qamar, U. Naeem, S. Khan, and M. Chongcheawchamnan, "Shafique MF mutual coupling reduction for high-performance densely packed patch antenna arrays on finite substrate," *IEEE Transactions on Antennas and Propagation*, vol. 64, no. 5, pp. 1653-1660, 2016.
- [20] K. Yu, Y. Li, and X. Liu, "Mutual coupling reduction of a MIMO antenna array using 3-D novel

- meta-material structures,” *Applied Computational Electromagnetics Society Journal*, vol. 33, no. 7, pp. 758-763, 2018.
- [21] M. Farahani, J. Pourahmadazar, M. Akbari, M. Nedil, A. Sebak, and T. Denidni, “Mutual coupling reduction in millimeter-wave MIMO antenna array using a metamaterial polarization-rotator wall,” *IEEE Antennas and Wireless Propagation Letters*, vol. 16, pp. 2324-2327, 2017.
- [22] D. Binion, P. Werner, D. Werner, E. Lier, and T. Hand, “Metamaterial enhanced antenna systems: A review,” *2018 International Applied Computational Electromagnetics Society Symposium (ACES)*, Denver, CO, USA, Mar. 2018.
- [23] Y. Liu, Y. Hao, H. Wang, K. Li, and S. Gong, “Low RCS microstrip patch antenna using frequency-selective surface and microstrip resonator,” *IEEE Antennas and Wireless Propagation Letters*, vol. 14, pp. 1290-1293, 2015.
- [24] M. Pazokian, N. Komjani, and M. Karimipour, “Broadband RCS reduction of microstrip antenna using coding frequency selective surface,” *IEEE Antennas and Wireless Propagation Letters*, vol. 17, no. 8, pp. 1382-1385, 2018.
- [25] R. Dickie, S. Christie, R. Cahill, P. Baine, V. Fusco, K. Parow-Souchon, M. Henry, P. G. Huggard, R. S. Donnan, O. Sushko, R. Dubrovka, C. G. Parini, and V. Kangas, “Low-pass FSS for 50–230 GHz quasi-optical demultiplexing for the metop second-generation microwave sounder instrument,” *IEEE Transactions on Antennas and Propagation*, vol. 65, no. 10, pp. 5312-5321, 2017.
- [26] R. Dickie, R. Cahill, H. Gamble, V. Fusco, A. Schuchinsky, and N. Grant, “Spatial demultiplexing in the submillimeter wave band using multilayer free-standing frequency selective surfaces,” *IEEE Transactions on Antennas and Propagation*, vol. 53, no. 6, pp. 1904-1911, 2005.
- [27] D. Xie, X. Liu, H. Guo, X. Yang, C. Liu, and L. Zhu. “A wideband absorber with a multiresonant gridded-square FSS for antenna RCS reduction,” *IEEE Antennas and Wireless Propagation Letters*, vol. 16, pp. 629-632, 2017.
- [28] M. Li, S. Xiao, Y. Bai, and B. Wang, “An ultrathin and broadband radar absorber using resistive FSS,” *IEEE Antennas and Wireless Propagation Letters*, vol. 11, pp. 748-751, 2012.
- [29] K. Wu, C. Wei, X. Mei, and Z. Zhang, “Array-antenna decoupling surface,” *IEEE Transactions on Antennas and Propagation*, vol. 64, no. 12, pp. 6728-6738, 2017.
- [30] J. Guo, F. Liu, L. Zhao, G. Huang, and Y. Li, “Meta-surface antenna array decoupling designs for two linear polarized antennas coupled in H-plane and E-plane,” *IEEE Access*, vol. 7, pp. 100442-100452, 2019.
- [31] F. Liu, J. Guo, L. Zhao, X. Shen, and Y. Yin, “A meta-surface decoupling method for two linear polarized antenna array in sub-6 GHz base station applications,” *IEEE Access*, vol. 7, pp. 2759-2768, 2019.
- [32] D. Smith and S. Schultz, “Determination of effective permittivity and permeability of metamaterial from reflection and transmission coefficients,” *Physical Review B*, vol. 65, pp. 195104.1-195104.5, 2002.
- [33] F. Liu, J. Guo, L. Zhao, G. L. Huang, Y. Li, and Y. Yin, “Ceramic superstrate-based decoupling method for two closely packed antennas with cross-polarization suppression,” *IEEE Transactions on Antennas and Propagation*, vol. 69, no. 3, pp. 1751-1756, 2021.
- [34] J. Jiang, Y. Xia, and Y. Li, “High isolated X-band MIMO array using novel wheel-like metamaterial decoupling structure,” *Applied Computational Electromagnetics Society Journal*, vol. 34, no. 12, pp. 1829-1836, 2019.
- [35] J. Jiang, Y. Li, L. Zhao, and X. Liu, “Wideband MIMO Directional antenna array with single-layered meta-material decoupling structure for X-band application,” *Applied Computational Electromagnetics Society Journal*, vol. 35, no. 5, 2020.
- [36] X. Huang, Y. Li, Y. Zakharow, and B. Chen, “Affine projection Lorentzian algorithm for vehicle hands-free echo cancellation,” *IEEE Transactions on Vehicular Technology*, 10.1109/TVT.2021.3061126, 2021.
- [37] T. Liang, Y. Li, W. Xue, Y. Li, and T. Jiang, “Performance and analysis of recursive constrained least Lncosh algorithm under impulsive noises,” *IEEE Transactions on Circuits and Systems II: Express Briefs*, 10.1109/TCSII.2020.3037877, 2021.
- [38] W. Shi, Y. Li, and Y. Wang, “Noise-free maximum correntropy criterion algorithm in non-gaussian environment,” *IEEE Transactions on Circuits and Systems II: Express Briefs*, vol. 67, no. 10, pp. 2224-2228, Oct. 2020.
- [39] Y. Li, Z. Jiang, W. Shi, X. Han, and B. D. Chen, “Blocked maximum correntropy criterion algorithm for cluster-sparse system identification,” *IEEE Transactions on Circuits and Systems II: Express Briefs*, vol. 66, no. 11, pp. 1915-1919, 2019.